A SPATIALLY RESOLVED EGFR SIGNALING MODEL PREDICTS THE LENGTH SCALE OF GAB1-SHP2 COMPLEX PERSISTENCE

Paul J. Myers[1,†], Christopher M. Furcht[2,†,#], Itziar Pinilla-Macua[3], Alexander Sorkin[3], William M. Deen[4], Matthew J. Lazzara[1,5]

[1]Department of Chemical Engineering, [5]Department of Biomedical Engineering
University of Virginia, Charlottesville, VA

[2]Department of Chemical and Biomolecular Engineering,
University of Pennsylvania, Philadelphia, PA

[3]Department of Cell Biology, University of Pittsburgh, Pittsburgh, PA

[4]Department of Chemical Engineering, Massachusetts Institute of Technology, Cambridge, MA

[†]These authors contributed equally to this work.
[#]Current Address: Bristol Myers Squibb, Summit, New Jersey, United States of America

Running Title: EGFR spatiotemporal activation of SHP2

Keywords: reaction-diffusion, kinase, phosphatase, sensitivity analysis, proximity ligation assay

Corresponding author:
Matthew J. Lazzara
385 McCormick Road
Charlottesville, VA 22903
Phone: 434-243-9767
E-mail: mlazzara@virginia.edu

ABSTRACT

Activation of receptor tyrosine kinases (RTKs) promotes the intracellular assembly of protein complexes formed through phosphotyrosine-SH2 domain linkages. These interactions are weak and reversible, and the dephosphorylation of uncomplexed phosphorylated proteins can be rapid enough to reduce the time and length scales of protein complex persistence distal from the receptor. This limitation may be overcome by cytosolic kinases that rephosphorylate constituent complex proteins as they diffuse. To develop quantitative understanding of the spatiotemporal regulation of these processes, we generated a reaction-diffusion model describing how membrane-bound epidermal growth factor receptor (EGFR) activates the SH2 domain-containing protein tyrosine phosphatase SHP2 by assembling SHP2 complexes with the adaptor GRB2-associated binder 1 (GAB1). Src family kinases (SFKs) were included as a diffusible EGFR-activated intermediary kinase for GAB1. Contrary to the textbook picture of EGFR-mediated SHP2 activation, the model predicts that GAB1-SHP2 complexes can remain intact distal from membrane-retained EGFR at ~80% of their plasma membrane concentration over the entire intracellular length scale. Parameter sensitivity analysis identified SFK inactivation as one of the most important kinetic processes controlling GAB1-SHP2 spatial persistence, revealing the key role of repeated adaptor phosphorylation in maintaining SHP2 activity. A simple order of magnitude analysis of the controlling rate processes supports the predictions of the coupled differential equation model. Furthermore, proximity ligation assays and immunofluorescence microscopy in carcinoma cells demonstrate that GAB1-SHP2 complexes are increasingly cytoplasmic and distal from EGFR as time proceeds after acute EGFR activation, consistent with model predictions. These results provide quantitative insight into a mechanism that may be alternately tuned for different receptors and downstream effector complexes to enable receptor control of signaling at a distance.

STATEMENT OF SIGNIFICANCE

The textbook understanding of receptor-mediated signaling involves the assembly of protein complexes at the receptor cytosolic tail and complex movement within the cell by protein trafficking. However, reaction-diffusion processes can also play an important role in distributing signaling proteins throughout the cell, potentially quite distal from signal-initiating receptors. Indeed, receptors can activate cytosolic kinases that may maintain the phosphorylation-dependent complexation of downstream effector complexes through many rounds of complex dissociation and protein dephosphorylation. Here, we develop quantitative understanding of this mode of signal regulation through development of a mechanistic computational model and demonstrate, with experimental validation, that membrane-bound receptors can regulate signaling through downstream effector complexes over the entire intracellular length scale.

INTRODUCTION

Cell signaling by receptor tyrosine kinases (RTKs) involves the recruitment of SH2 and PTB domain-containing cytosolic adapter proteins to phosphorylated receptor cytoplasmic tyrosines. Phospho-dependent linkages between receptors and adapters and among proteins in larger complexes nucleated upon receptor activation are highly reversible, with low micromolar affinities and dissociation kinetics so rapid that complexes must reform repeatedly to sustain signaling (*1*, *2*). Protein tyrosine phosphatase (PTP) activity is also high enough that phosphotyrosines on constituent proteins can be appreciably dephosphorylated while not protected by SH2 domains (*3*, *4*). These effects may limit the access of functional, intact protein complexes to some intracellular locations, even though protein diffusion time scales are small (~10 sec).

While some protein complexes form in direct association with signal-initiating receptors (*5*), RTKs also activate cytosolic kinases that can promote the persistent complexation of proteins distal from the membrane. These effects can be hidden but present in co-immunoprecipitation experiments. Indeed, the presence of an RTK in the pulldown of a complex of downstream effectors does not necessarily indicate that all effector complexes are RTK-bound. However, the intracellular length scale over which intermediary RTK-activated kinases can maintain intact protein complexes and the most important determinants of that length scale are unknown. Here, we investigate this type of signaling regulation for the epidermal growth factor receptor (EGFR) and downstream protein complexes containing SH2 domain-containing phosphatase 2 (SHP2) and GRB2-associated binder 1 (GAB1).

SHP2 is encoded by the proto-oncogene *PTPN11* and is required for complete activation of ERK downstream of most RTKs (*6*-*8*). SHP2 is basally catalytically inhibited by an intramolecular interaction between its N-terminal SH2 domain and its phosphatase domain (*9*), but this tethering is relieved when SHP2 N- and C-terminal SH2 domains engage phosphorylated

tyrosines including GAB1 Y627 and Y659 (*10*). Thus, GAB1-SHP2 complexes represent an active form of SHP2. In response to EGFR activation, GAB1 is phosphorylated by Src family kinases (SFKs), which reside both at the membrane and in the cytoplasm (*10-12*). SHP2 binding to GAB1 has conventionally been viewed as a recruitment of cytosolic SHP2 to the plasma membrane through RTK-containing complexes such as EGFR-GRB2-GAB1-SHP2 (*13*) or through binding to PIP_3-bound GAB1 (*14*). RTKs including Ret, HER2, and MET can also recruit SHP2 to the plasma membrane (*15-17*). Interestingly, MET promotes more substantial SHP2 redistribution toward the plasma membrane than EGFR (*18*). This difference may be based in part on the ability of EGFR to maintain cytosolic GAB1-SHP2 complexes by repeated SFK-mediated GAB1 phosphorylation (*12*). Importantly, the ability for SFKs to phosphorylate cytosolic GAB1 will be influenced by the spatiotemporal regulation of SFK activity. SFKs can be activated at the plasma membrane in response to EGFR activation (*19-23*), and they are inactivated throughout the cell by PTPs and c-SRC kinase-mediated phosphorylation of negative regulatory tyrosines on SFKs (*24*). Based on this, SFK activity may rapidly decline distal from the plasma membrane.

Here, we develop a reaction-diffusion model to predict the temporal and spatial persistence of GAB1-SHP2 complexes in EGF-treated cells containing plasma membrane and cytosolic compartments. The fitted model predicts that GAB1-SHP2 complexes persist at nearly 80% of their plasma membrane concentration over the entire intracellular length scale. That is, EGFR in the plasma membrane can drive the activity of SHP2 throughout the cell interior. A parameter sensitivity analysis reveals that this complex persistence depends strongly on rates of SHP2-GAB1 association and dissociation, SFK inactivation, and GAB1 dephosphorylation. Model predictions are supported by a simple order of magnitude analysis of the competing reaction and diffusion processes and by experimental measurements based on proximity ligation assays and

immunofluorescence microscopy. Our results demonstrate that cytosolic SFK activity enables EGFR to maintain active GAB1-SHP2 complexes throughout the intracellular domain and establish a quantitative framework for considering related phenomena in other receptor systems and cell settings.

METHODS

Model Development

General model description. Model equations comprise a system of coupled ordinary and partial differential equations for membrane and cytosolic species, respectively. Equations account for protein diffusion, reversible binding, and reversible tyrosine phosphorylation among EGFR, SFKs, GRB2, GAB1, and SHP2 in a spherical cell with radius R. Reaction rate expressions follow mass action kinetics. A model schematic is provided in Fig. 1, and model parameters are summarized in Table 1.

Cytosolic species. Within the cytosolic compartment, conservation of species i (C_i) was modeled as

$$\frac{\partial C_i}{\partial t} = D_i \frac{1}{r^2} \frac{\partial}{\partial r}\left(r^2 \frac{\partial C_i}{\partial r} \right) + R_{Vi} \quad [1]$$

where D_i is the diffusivity and R_{Vi} is the net volumetric rate of generation. No-flux (symmetry) boundary conditions were implemented at the cell center for all species such that

$$\frac{\partial C_i}{\partial r}(0,t) = 0 \quad [2]$$

Robin boundary conditions were applied at the membrane to equate the diffusive flux from the membrane (into the cytosol) to the rate of generation of species i (R_{si}) at the membrane. Thus,

$$D_i \frac{\partial C_i}{\partial r}(R,t) = R_{Si} \quad [3]$$

Membrane species. Membrane species were treated as uniformly distributed in the membrane and modeled only as a function of time as

$$\frac{dC_i}{dt} = R_{Si} \quad [4]$$

Finite difference solution. Partial differential equations were discretized using an explicit finite difference method, wherein first- and second-order derivatives were approximated using forward and central differences, respectively. At each time point, the system of algebraic equations resulting from discretizing over the entire spatial domain was explicitly solved using concentrations from the prior time point. The coupled equations for membrane proteins and boundary conditions for cytosolic proteins were simultaneously solved using the semi-implicit Euler method. Discretized boundary conditions for cytosolic proteins were evaluated first, using initial guesses for membrane protein concentrations at the next time step. Subsequently, discretized conservation equations for membrane proteins were evaluated using cytosolic protein concentrations from the explicit finite difference calculation. The membrane protein concentrations calculated in this step were then used as initial guesses for the boundary conditions in the next iteration of the semi-implicit scheme. This process was repeated iteratively until the fractional error between the previous and updated concentrations for membrane species and cytosolic proteins at the boundary was $< 1\times10^{-6}$. The process above was then successively repeated for each time point until the end of the time domain considered was reached. Additional details are provided in Appendix S1.

Simplified, steady-state model. A simplified steady state model was developed by limiting the role of EGFR to SFK activation only (i.e., no adaptor binding) and setting the concentration of phosphorylated EGFR to the value predicted by the full model for the 5-min response to EGF. Solving the conservation equations for active and inactive SFKs analytically, the *r*-dependent concentration of active SFKs is

$$C_{SFK,a}(r) = \frac{k_{S,a}C_{pE,tot}C_{o,SFK}}{D_{SFK}}\left[\frac{\cosh mr}{R} + \frac{\sinh mr}{mR}\left(\frac{k_{S,a}C_{pE,tot}}{D_{SFK}} - \frac{1}{R}\right)\right]^{-1}\frac{\sinh mr}{mr} \qquad [5]$$

where C_{pE} is the concentration of phosphorylated EGFR, and other parameters are as defined in Table 1. The concentration of inactive SFKs is $C_{SFK,i} = C_{o,SFK} - C_{SFK,a}$, where $C_{o,SFK}$ is the initial concentration of SFKs.

Without binding to EGFR and GRB2 at the cell membrane, the boundary conditions for the four remaining cytosolic species (GAB1, pGAB1, pGAB1-SHP2, and SHP2) are of the form

$$\frac{\partial C_i}{\partial r}(0,t) = \frac{\partial C_i}{\partial r}(R,t) = 0 \qquad [6]$$

Subject to Eq. [6], the conservation equations for these species were solved using a modified, steady-state finite difference method without time steps.

To create a further simplified model, the governing equations for GAB1, pGAB1, pGAB1-SHP2, and SHP2 were reduced to just two equations for pGAB1 and pGAB1-SHP2 using conserved scalar quantities. The resulting equations were solved using the modified finite difference scheme. Finally, the system was reduced yet further to a single conservation equation for pGAB1 by assuming that GAB1 and SHP2 binding was everywhere at equilibrium, which enabled the elimination of all other species from the differential equation by substitution. The resulting conservation equation for pGAB1 was also solved by modified finite difference. Appendix S2 provides additional details on model simplifications, governing equations, and the modified steady-state finite difference approach.

Model Implementation

General considerations. Model codes were written and compiled primarily in MATLAB 2020b and Julia v1.6.5 and are available on GitHub under the username "LazzaraLab." In total, the model consists of 18 distinct protein species (10 cytosolic and eight membrane) and 25 reactions. Model parameters are described in Table 1. For all finite difference calculations, except

those for sensitivity analyses, the spatial dimension was discretized using a step = 0.1 μm. For sensitivity analyses, a step = 0.2 μm was used to increase calculation efficiency. For all calculations, the time step was set based on the explicit finite difference stability criterion described in Eq. [8] by Bieniasz (*25*) for diffusion problems with homogeneous reactions. Typical time steps ranged between ~3×10^{-4} sec to ~3×10^{-6} sec, depending on the values of model parameters and the spatial step size.

An additional version of the model was developed in Virtual Cell (VCell) (*26*, *27*) to provide accessibility to VCell users. The VCell model "Myers&Furcht_spatial_GAB1_SHP2" was constructed as a BioModel in VCell 7.1 and is available in the public domain through the Public BioModels portal in VCell and at http://vcell.org/vcell-models under the shared username "LazzaraLab." Solution geometries were constructed in VCell by defining the cytoplasmic volume compartment as a sphere with a radius of 10 μm or 50 μm.

Representative cell. *R* was set equal to 10 μm (*28*) for most calculations. When the model was used to compute length scales for species persistence that could exceed 10 μm (e.g., with perturbed parameters), *R* was set to 50 μm. For most calculations, EGFR, GRB2, GAB1, SHP2, and SFKs were assumed to be at cellular concentrations of 6×10^5 per cell, as described in a previous, purely dynamic model (*12*). However, in some calculations, stoichiometries based on absolute quantification of protein in cell lines were used. Total concentrations of EGFR, SFKs, GRB2, GAB1, and SHP2 were converted to units of molecules/μm^3 using the appropriate volume and surface area conversion factors such that the total number of molecules of each protein per cell did not change between calculations whether the cell radius was set to 10 or 50 μm.

Kinetic processes considered and model parameterization. EGF binding at the plasma membrane was modeled as a reversible process characterized by association (*29*) and dissociation

(*30*) rate constants. EGF was treated as present at a constant concentration of 10 ng/mL, which is approximately equal to EGF's affinity for EGFR. The EGFR dimerization rate constant was used as calculated previously (*31*). Dimer uncoupling rate constants in the presence of EGF were described previously. All dimer species were assumed to be symmetric, i.e., no coupling of ligand-bound and -unbound EGFR monomers. EGFR phosphorylation was modeled as occurring between EGF-bound EGFR receptors in a dimer, where both receptors are simultaneously phosphorylated at a representative tyrosine (Y1068) that binds GRB2. EGFR dephosphorylation was modeled as zeroth order based on a previously described rate constant (*12*).

As in prior work (*12, 32*), SFK activation was modeled as a first-order process wherein phosphorylated EGFR activates SFK at the plasma membrane. This approach is based on knowledge that Src SH2 domains can bind EGFR (*33*) and that Src SH2 engagement promotes autophosphorylation and activation of Src (*34*). SFK inactivation was modeled as zeroth order volumetric process occurring throughout the cytosol.

GAB1 phosphorylation at a representative tyrosine that binds SHP2 (e.g., Y627) was modeled as a process catalyzed by active SFKs throughout the cytosol. GAB1 dephosphorylation was modeled as a zeroth order volumetric reaction in the cytosol. Binding interactions among GRB2, GAB1, and SHP2 were modeled as described previously (*12*).

Diffusivities for cytosolic proteins and complexes were based on the diffusivity of tubulin (*35*) and an adjustment factor based on differences in the hydrodynamic radii of tubulin and a given protein monomer or complex. The hydrodynamic radii of protein monomers and complexes were estimated based on their molecular weights (*36*). See Appendix S4 for details.

Parameter fitting. Parameters for SFK activation/inactivation and GAB1 phosphorylation/dephosphorylation were fit by matching model predictions to purely dynamic

predictions for EGF-induced pGAB1 and active SFKs from a prior model (*12*). Specifically, k_{G1p}, k_{G1dp}, $k_{S,a}$, and $k_{S,i}$ were fit by matching the predicted spatially averaged [pGAB1] and [aSFK] in the present model to prior predictions for [pGAB1] and [aSFK]. The *particleswarm* function in MATLAB was used to fit the parameters by minimizing the sum-of-squares error between the present and prior model results. The best-fit results are included in Table 1. The fitted model accurately recapitulates the previously predicted dynamics of SFK activation and GAB1 phosphorylation in response to EGF (Fig. S1A).

Sensitivity analysis. Model sensitivity to simultaneous changes in all parameter values was computed using the extended Fourier amplitude sensitivity test (eFAST) (*37*, *38*). eFAST calculates total-order sensitivity indices (S_T), which indicate the fraction of the overall model output variance that can be attributed to variations in an input parameter of interest when perturbing all parameters simultaneously. eFAST calculations were performed with the Julia version of the model using the GlobalSensitivity.jl package. Diffusivities and kinetic parameters were varied by a factor ≤ 10 above or below their base values. Protein concentrations were allowed to vary between 100 and 1,000,000 molecules per cell. In all eFAST calculations, 1,000 simulations were run per varied model parameter.

Length scales for active SFKs and GAB1-SHP2 complexes

Estimates for the length scales over which concentrations of active SFKs and GAB1-SHP2 complexes change were developed by considering the orders of magnitude of the rate processes involved in the reaction-diffusion mechanism. The length scale obtained for GAB1-SHP2 was assumed to apply to GRB2-GAB1-SHP2 because the diffusivities of these two species are nearly

identical (Table 1) and GRB2 binding does not prevent GAB1-SHP2 association in the current model topology. See Appendix S3 for additional details regarding these derivations.

The length scale of active SFKs can be derived from the steady conservation equation for $C_{SFK,a}$, which is

$$D_{SFK}\frac{1}{r^2}\frac{d}{dr}\left(r^2\frac{dC_{SFK,a}}{dr}\right)-k_{S,i}C_{SFK,a}=0 \quad [7]$$

Note that R_{Vi} for active SFKs does not include a forward (activation) rate because SFK activation occurs only at the plasma membrane. Dimensionless $C_{SFK,a}$ and r are defined as

$$\theta=\frac{C_{SFK,a}}{C_{o,SFK}} \quad [8]$$

$$\eta=\frac{r}{R} \quad [9]$$

Substituting these definitions into Eq. [7] yields

$$\frac{1}{\eta^2}\frac{d}{d\eta}\left(\eta^2\frac{d\theta}{d\eta}\right)=\mathrm{Da}\,\theta \quad [10]$$

where the Damköhler number Da = $k_{S,i}R^2/D_{SFK}$ is a dimensionless quantity describing the competition between SFK inactivation and SFK diffusion.

Based on the parameter values in Table 1, Da ≈ 40. Thus, the inactivation of SFKs occurs rapidly compared to SFK diffusion over the length scale R, and a sharp gradient in $C_{SFK,a}$ is expected. The large value of Da also indicates that Eq. [10] is not properly scaled (i.e., not all terms are ~1), which is a consequence of the geometric length R (used to define η) overestimating the length scale for changes in $C_{SFK,a}$. Redefining the radial coordinate by incorporating Da as

$$\chi=\eta\mathrm{Da}^{1/2}=r\left(\frac{k_{S,i}}{D_{SFK}}\right)^{1/2} \quad [11]$$

eliminates Da from the conservation equation, resulting in this scaled result:

$$\frac{1}{\chi^2}\frac{d}{d\chi}\left(\chi^2\frac{d\theta}{d\chi}\right)=\theta \qquad [12]$$

Based on Eq. [11], the length scale for changes in $C_{SFK,a}$ ($\delta_{SFK,a}$) is

$$\delta_{SFK,a} \sim \left(\frac{D_{SFK}}{k_{S,i}}\right)^{1/2} \qquad [13]$$

where "~" denotes order-of-magnitude equality.

While $\delta_{SFK,a}$ is readily derived through standard scaling analysis (*39*), the length scale for GAB1-SHP2 complex persistence (δ_{G1S2}) is more challenging to obtain due to the coupled kinetic processes involved. An alternative approach is to estimate and sum the length scales for the processes that cooperate to determine δ_{G1S2}: i. SFK-mediated GAB1 phosphorylation, ii. GAB1-SHP2 dissociation, and iii. GAB1 dephosphorylation. This approach recognizes that complexes will form wherever GAB1 is actively being phosphorylated, that intact complexes require a finite time to dissociate, and that complexes can reform where GAB1 remains phosphorylated.

The length scale for SFK-mediated GAB1 phosphorylation is just $\delta_{SFK,a}$. Based on the same reasoning used to derive $\delta_{SFK,a}$, the length scale for GAB1-SHP2 dissociation (δ_{dis}) is

$$\delta_{dis} \sim \left(\frac{D_{G1S2}}{k_{S2,off}}\right)^{1/2} \qquad [14]$$

and the length scale for GAB1 dephosphorylation (δ_{dep}) is

$$\delta_{dep} \sim \left(\frac{D_{G1}}{k_{G1do}}\right)^{1/2} \qquad [15]$$

Thus, δ_{G1S2} can be estimated as

$$\delta_{G1S2} \sim \left(\frac{D_{SFK}}{k_{S,i}}\right)^{1/2} + \left(\frac{D_{G1S2}}{k_{S2,off}}\right)^{1/2} + \left(\frac{D_{G1}}{k_{G1dp}}\right)^{1/2} \qquad [16]$$

Experimental Methods

Cell culture. Gene-edited HeLa cells expressing mVenus-HRAS (HeLa/mV-HRAS) from a single endogenous *HRAS* locus were described previously (*40*). Unless otherwise noted, cells were cultured in Dulbecco's Modified Eagle's Medium (DMEM) supplemented with 10% fetal bovine serum (FBS) (Avantor), 1% penicillin-streptomycin (10,000 µg/mL), and 1% L-glutamine (200 mM). Cells were confirmed to be mycoplasma-negative using the MycoAlert Mycoplasma Detection Kit (LT07-318, Lonza).

Proximity ligation assay and immunofluorescence. HeLa/mV-HRAS cells were plated on 12-mm coverslips in six-well tissue culture dishes at 3×10^5 cells per well. ~24 hr after plating, cells were serum-starved by switching them to DMEM containing 0.1 % FBS for at least 16 hr. Serum-starved cells were treated with recombinant human EGF (PeproTech AF-100-15) at 10 ng/mL for ≤ 15 min. Medium was then aspirated, and cells were fixed in 4% paraformaldehyde in PBS for 20 min, followed by permeabilization with 0.25% Triton X-100 in PBS for 5 min. Coverslips were blocked in Duolink Blocking Solution (Sigma Aldrich) for 1 hr at 37°C and were then incubated with primary antibodies overnight at 4°C. All antibodies were diluted in Odyssey Blocking Buffer (OBB). For GAB1-SHP2 proximity ligation assays (PLA), mouse SHP2 antibody (sc-7384, Santa Cruz Biotechnology, 1:50) and rabbit GAB1 antibody (HPA049599, Sigma-Aldrich, 1:50) were used. For EGFR-GRB2 PLA, mouse EGFR antibody (CST D381B, Cell Signaling Technology, 1:100) and rabbit GRB2 antibody (BD 610111, BD Biosciences, 1:100) were used. PLA probes were anti-rabbit PLUS (DUO92002, Sigma-Aldrich) and anti-mouse MINUS (DUO92004, Sigma-Aldrich) and were used and detected using Duolink In Situ Far Red Detection Reagents (Sigma-Aldrich) according to the manufacturer's instructions. After staining with PLA probes, coverslips were incubated overnight at 4°C with rat EGFR antibody (ab231,

Abcam, 1:200). EGFR was detected by incubating coverslips for 1 hr at 37°C with anti-rat Alexa Fluor 594 (A-11007, Invitrogen, 1:750) and Hoechst nuclear stain (1:2000). Coverslips were mounted on glass slides using ProLong Gold Antifade Mounting Medium (Thermo Fisher, P36930). Epifluorescence images were obtained with a Zeiss AxioObserver Z1 using 20×, 40× oil immersion, and 63× oil immersion objective lenses.

Fluorescence images were analyzed using the FIJI distribution of ImageJ (*41*). Quantification of PLA puncta and colocalization of PLA and EGFR puncta was performed using custom ImageJ macros that were written using a combination of the puncta quantification processing steps described by Horzum et al. (*42*) and the object-based colocalization analysis steps described by Moser et al. (*43*). Briefly, maximum-intensity z-projections of PLA and EGFR immunofluorescence (IF) images were first background-corrected using the rolling ball algorithm, followed by local contrast enhancement using contrast-limited adaptive histogram equalization (*44*) via the CLAHE ImageJ plugin. Background was further corrected by applying the exponential filter, followed by automatic adjustment of the brightness and contrast. The Laplacian of Gaussian (LoG) filter was then applied to enhance individual puncta. LoG-filtered images were then thresholded to identify individual PLA and EGFR puncta, which were then related based on object overlap to determine signal colocalization. Individual nuclei were identified by thresholding background-subtracted and histogram-equalized nuclear stain images.

RESULTS

Base Model Predictions

As detailed in *Methods*, the model accounts for EGFR phosphorylation, SFK activation, GAB1 phosphorylation, and GAB1-SHP2 complex formation in a spherical cytosolic compartment bounded by a plasma membrane (Figure 1). Unless otherwise stated, the concentration of GAB1-SHP2 complexes is calculated as the sum of the species pGAB1-SHP2 and GRB2-pGAB1-SHP2. Simulations were limited to a 5-min response to EGF because peak EGFR activation and adapter binding typically occur within this time (*45, 46*) and because EGFR endocytosis and degradation are prominent after 5 min (*5, 40, 47, 48*). Thus, model calculations provide a conservative estimate of the ability of the membrane-localized receptors to regulate signaling via SHP2 throughout the cytoplasmic domain.

The full model predicts that SFKs rapidly activate at the plasma membrane in response to EGF but that the concentration of active SFKs decays substantially over a length scale that is small compared to the cell radius. In contrast, the concentration of pGAB1 decays only modestly moving away from the membrane and toward the cell interior (Figs. 2, A and B). The difference between the length scales for active SFKs and pGAB1 decay is related in part to the time required for GAB1 dephosphorylation, an issue examined in greater detail later. The difference in length scales is also related to an effective signaling amplification step from EGFR to GAB1, wherein ~2 pGAB1 molecules result via SFK for every pEGFR (Fig. 2C). As with pGAB1, the abundance of GAB1-SHP2 complexes is largely unchanged as a function of the radial coordinate *r*, suggesting that SHP2 remains active over the entire intracellular length scale when activated by membrane-retained EGFR (Fig. 2D). The predicted response of GAB1-SHP2 complexes to treatment with the EGFR inhibitor gefitinib after an initial pulse of EGF demonstrated a slower decay of GAB1-SHP2

complexes (~2 min; Fig. 2E) than the rate of initial complex formation (~30 sec; Fig. 2D). The slower rate of decay is the result of the time scale required for GAB1 dephosphorylation, which cannot occur until the effect of EGFR inactivation propagates to an inactivation of SFKs. The finite time scale for this propagation explains why the predicted loss of EGFR activity occurs more quickly than does the loss of GAB1-SHP2 complexes.

The robustness of the GAB1-SHP2 length scale prediction was tested by creating 1,000 parameter sets in which each parameter was randomly perturbed by up to an order of magnitude (up or down) from its base value. For > 90% of the 1,000 parameter sets, the concentration of GAB1-SHP2 complexes at the cell center is ≥ 50% of the GAB1-SHP2 concentration at the cell surface, and virtually all parameter sets meet less stringent thresholds for complex persistence (Fig. 2F). Therefore, the model prediction of GAB1-SHP2 complexes being maintained distal from the cell surface appears robust even if the model parameters are not well estimated.

Calculations made using a Virtual Cell (VCell) implementation of the full reaction-diffusion model are consistent with predictions of the model obtained using MATLAB and Julia (Fig. S1, B-D). Accessibility of this model is described in *Methods* for VCell users.

Steady-state Model Predictions

Predictions of the full model were compared to a simplified steady model in which EGFR was considered only for its ability to activate SFKs, with the abundance of pEGFR chosen as that predicted by the full model for a 5-min response to 10 ng/mL EGF. See *Methods* for details. Solutions for active and inactive SFKs matched the solutions from the full reaction-diffusion model nearly identically (Fig. S2A). Predictions of the simplified model for GAB1-SHP2, pGAB1, GAB1, and SHP2 agreed with predictions of the full model to within ~15% error or less (Fig. S2

B-E). In addition to supporting the conclusion that the length scale for GAB1-SHP2 complex persistence is $\geq R$, these results demonstrate that the GAB1-SHP2 complexes are governed by nearly pseudo-steady behavior with respect to EGFR dynamics. The results also demonstrate that GRB2-GAB1 binding, which was neglected in the simplified model, has little influence on GAB1-SHP2 complex persistence.

Parameter Sensitivity Analysis

To identify rate processes that strongly influence the concentration and distribution of GAB1-SHP2 complexes, the extended Fourier amplitude sensitivity test (eFAST) approach was used to conduct a multivariate parameter sensitivity analysis. Model parameters were varied by up to a factor of 10, and a 5-min response to 10 ng/mL EGF was considered (Fig. 3A). The average GAB1-SHP2 concentration was most sensitive to perturbations to SHP2 binding to ($k_{S2,f}$) and unbinding from GAB1 ($k_{S2,r}$). To determine parameters that control the distribution of GAB1-SHP2 complexes, we calculated the distance from the cell surface where the concentration of GAB1-SHP2 reaches 50% of its membrane value ($r_{1/2}$). $r_{1/2}$ was most sensitive to changes in the dephosphorylation kinetics of GAB1 (k_{G1dp}) and the diffusivities of GAB1 and pGAB1-SHP2. $r_{1/2}$ was also sensitive, to a lesser degree, to changes in SHP2 binding kinetics and the diffusivity and inactivation kinetics of SFKs (D_{SFK} and $k_{S,i}$, respectively). The ratio of GAB1-SHP2 at the cell center versus cell surface was sensitive to the same perturbations. Consistent with results in Fig. S2, perturbations to rate constants governing EGFR-GRB2 interactions had little effect on GAB1-SHP2 complex abundance or persistence. Univariate perturbations to the most important parameters from the eFAST analysis confirmed their relative influence on the spatial distribution of GAB1-SHP2 complexes and demonstrated expected qualitative trends (Fig. 3, B-E). For

example, a 10-fold increase in k_{G1dp} limited the concentration of GAB1-SHP2 at the cell center to just 25% of its value at the membrane.

We next determined the model's sensitivity to perturbations in initial protein concentrations, again using the eFAST approach. This analysis revealed that the center-to-surface ratio of GAB1-SHP2 was highly sensitive to changes in SHP2 expression yet only mildly sensitive to changes in SFK expression (Fig. 3F). Indeed, perturbations to SFK expression alone result in relatively modest changes to GAB1-SHP2 complex distribution (Fig. 3G). This result was surprising given that GAB1-SHP2 complex persistence depends strongly on the diffusivity and inactivation rate of SFKs (Fig. 3A) and that a purely dynamic model is highly sensitive to changes in SFK expression (*12*). We investigated this further by analyzing whether SFK overexpression could compensate for increases in SFK inactivation and GAB1 dephosphorylation when determining the length scale for GAB1-SHP2 complex persistence. A ten-fold increase in SFK abundance can substantially offset the effect of an elevated GAB1 dephosphorylation rate (Fig. 3H), but the same increase cannot offset a faster rate of SFK inactivation. This observation is most likely explained by the fact that the length scale for active SFKs—which directly affects the length scale of GAB1-SHP2 persistence—is independent of concentration but not the rate of SFK inactivation. In the case of increased GAB1 dephosphorylation, the length scale for active SFKs remains unchanged, and SFK overexpression compensates by significantly increasing the average rate of GAB1 phosphorylation over the length scale where SFKs are active. Thus, increasing SFK expression can compensate for perturbations to the rate constants for some processes but not others. The characteristic length scales of actives SFKs and GAB1-SHP2 are described in further detail later.

Based on the protein concentration sensitivity analysis (Fig. 3F) and previously reported findings (*12, 49*), we next sought to determine if SHP2 binding could protect GAB1 from being dephosphorylated. While our previous purely dynamic model predicted little effect of SHP2 depletion or overexpression on GAB1 phosphorylation, the current spatially resolved model predicts that GAB1 phosphorylation is highly sensitive to changes in SHP2 expression (Fig. 3I). Indeed, the center-to-surface ratio of pGAB1 varied greatly in these simulations, ranging from 0.98 when SHP2 was overexpressed to as low as 0.48 when SHP2 was depleted, consistent with the results of Fig. 3F. This occurs because unbound and dephosphorylated GAB1 near the cell center is isolated from active SFKs. This physical separation, which is accounted for by the spatial model but ignored by a purely dynamic model, magnifies the protective effect of SHP2's binding on phosphorylated GAB1. Furthermore, SHP2 overexpression fully compensates for the effect of increasing the rate of GAB1 dephosphorylation or SFK inactivation on the persistence phospho-GAB1 (Fig. 3J). Based on these results, elevated SHP2 concentration can be expected to promote GAB1-SHP2 persistence by sustaining GAB1 phosphorylation through shielding it from phosphatases.

Effect of SFK Activity Confinement to the Membrane

While we and other investigators have found active SFKs in the cytosolic compartment (*12, 31*), some investigators report that active SFKs are confined primarily to the membrane due to palmitoylation or other post-translational modifications (*50*). To determine the effect of SFK compartmentalization on the GAB1-SHP2 persistence length scale, we set the diffusivity of active SFKs to nearly zero, confining their activity to the membrane. This change caused the center-to-surface ratio of GAB1-SHP2 to drop to ~0.61 compared to ~0.77 with the base model (Fig. 4A).

Overall, the persistence of GAB1-SHP2 was only moderately affected by confining SFK activity to the cell membrane. This occurs because $\delta_{SFK,a}$ is already small compared to R for the base model parameters. We next performed another eFAST analysis to determine whether the model parameter sensitivities changed due to active SFK membrane confinement (Fig. 4B). This version of the model was almost exclusively sensitive to the kinetics of GAB1 dephosphorylation and SHP2 binding to GAB1 and was entirely insensitive to the rate constants for SFK activation and inactivation. We assessed how much the rate constants for these processes needed to be varied to compensate for confinement of SFK activity to the cell membrane by performing model calculations over a range of values for the GAB1 dephosphorylation and GAB1-SHP2 dissociation rate constants (Fig. 4, C and D). These calculations indicated that a 0.5-fold change in the GAB1 dephosphorylation rate constant (k_{G1dp}) is sufficient to obtain the same ratio of center-to-surface GAB1-SHP2 as the base model and compensate for active SFK membrane confinement in the full spatiotemporal profile of GAB1-SHP2. For the rate of GAB1-SHP2 dissociation ($k_{S2,r}$), a 0.3-fold change from the base value was required to match the base model center-to-surface ratio of GAB1-SHP2, but we note that this change actually led to an overall increase in the cell-center concentration of cytosolic GAB1-SHP2 above that predicted by the base model. Thus, even if our base model assumption that active SFKs are diffusible is incorrect, relatively small adjustments to a small subset of model parameters can compensate for the effect SFK membrane confinement on GAB1-SHP2 persistence.

Estimating Length Scales by Order of Magnitude Analysis

To validate model predictions, we developed an independent estimate for the length scale of GAB1-SHP2 complex persistence based on scaling analyses of the conservation equations for

key species. The analysis is described in *Methods*, and the conceptual model describing why specific length scales were added is presented in Fig. 5A. Using the model parameter values in Table 1, the order of magnitude analysis predicts δ_{G1S2} ~ 5.4 μm, with approximately one-third of that determined by the length scale of which SFKs are active $\delta_{SFK,a}$ (~1.6 μm). Of the two remaining length scales that contribute to δ_{G1S2}, δ_{dep} is the larger (~2.8 μm) and δ_{dis} is the smaller (~1 μm) (Fig. 5B). The three-fold difference between δ_{dep} and δ_{dis} is consistent with results shown in Fig. 2, A and D.

We also compared the length scale estimates for active SFKs (Eq. [13]) and GAB1-SHP2 (Eq. [16]) against the model-predicted length scales $r_{1/2}$. Because $r_{1/2} \geq R$ for the base model, the cell radius was set to 50 μm for the calculations shown here. Length scales were calculated with base model parameters and for up to 10-fold variations, up or down, in the parameters included in Eq. [16] (Fig. 5C). The length scale predictions agreed well for both active SFKs and GAB1-SHP2. In all scenarios, $\delta_{SFK,a}$ is less than the cell radius R. The strong agreement indicates that Eqs. 13 and 16 capture the essential processes for determining the process length scales. Note that effects of cell curvature are neglected in our length scale estimates, and that curvature effects are anticipated to reduce δ by ~20-30% based on model calculations for spherical and rectangular coordinates (Fig. S3). Overall though, the length scale estimates generated concur with the predictions of the full model that GAB1-SHP2 complexes and support the conclusion that GAB1-SHP2 complexes persist over the entire intracellular length scale in response to EGFR activation.

Visualizing EGFR-driven GAB1-SHP2 complexes in carcinoma cells

To validate the central model prediction that GAB1-SHP2 complexes persist throughout the cell in response to EGFR activation, we used proximity ligation assays (PLA) and

immunofluorescence (IF) microscopy in HeLa cells and updated model calculations for known HeLa protein abundances. The stoichiometry and expression of pathway proteins in HeLa cells diverge substantially from the assumed expression levels in our base model (*51*). Notably, GAB1 is expressed at just ~1,500 copies/cell. Model calculations based on HeLa cell protein abundances nonetheless suggest that GAB1-SHP2 complexes should be distributed throughout the cell interior (Fig. 6, A-C) and that the length scale for complex persistence is nearly as large as predicted for the base model (Fig. 6D). This prediction is consistent with eFAST calculations showing that the model is primarily sensitive to changes in SHP2 expression but not other proteins (Fig. 3F). Since SHP2 is expressed in excess compared to GAB1 in HeLa cells (~300,000 versus ~1,500 molecules, respectively) and protects GAB1 from dephosphorylation, it is not surprising that the length scale of GAB1-SHP2 persistence is unchanged despite the low abundance of GAB1 in these cells. This prediction was again robust to simultaneous perturbations of all model parameters (Fig. 6E). Thus, the reaction-diffusion mechanism described by the model distributes even relatively small numbers of GAB1-SHP2 complexes throughout the cell interior. The equivalence of predicted length scales for the base model and HeLa protein abundances is consistent with the lack of species concentration dependence in the estimate for δ_{G1S2} in Eq. [16].

As a specific cell background for visualizing GAB1-SHP2 complexes relative to EGFR, we used gene-edited HeLa cells expressing an mVenus-HRAS fusion from one endogenous *HRAS* locus (*40*), which enables membrane visualization without use of stains. We first validated the use of PLA for determining the subcellular protein localization by performing EGFR-GRB2 PLA and immunofluorescence for EGFR (Fig. 7A). EGFR and GRB2 strongly associate upon EGFR phosphorylation. EGFR-GRB2 PLA signals should thus be almost entirely colocalized with an EGFR IF signal generated using an independent primary antibody. As expected, exogenous EGF

produced the obvious formation of EGFR-positive puncta by IF and EGFR-GRB2 PLA signals, each of which were visible throughout cells (Fig. 7, B and C). EGFR puncta form due to EGFR association with clathrin-coated pits and endocytosis, effects not explicitly considered in our model but described in more detail in the *Discussion*. PLA signals seen with primary antibody controls indicated that some of the apparent basal EGFR-GRB2 association in serum-starved cells may result from non-specific binding of PLA probes (Fig. S4A). Most importantly, colocalization analysis of EGFR-GRB2 PLA and EGFR IF signals indicated that nearly all EGFR-GRB2 puncta were colocalized with EGFR identified independently (Fig. 7, D and E). This result provides confidence in the ability of PLA to accurately represent the subcellular localization of protein complexes.

We next performed GAB1-SHP2 PLA and EGFR IF in parallel (Fig. 7F). As expected, exogeneous EGF produced clear GAB1-SHP2 PLA signals and EGFR puncta throughout the cells (Fig. 7G-H). Primary antibody controls indicated that the presence of low baseline PLA signal in serum-starved cells is likely due to a combination of some basal GAB1-SHP2 association and non-specific binding of the PLA anti-rabbit probe to epitopes in proximity to the SHP2 primary antibody. The observed increase in GAB1-SHP2 PLA signal with EGF is consistent with prior co-immunoprecipitation measurements (*12*). Quantitative image analysis revealed that the fraction of GAB1-SHP2 PLA puncta colocalizing with EGFR signal was substantially less than one and decreased over time (Fig. 7I). The difference was most prominent 15 min after EGF treatment, when only ~25% of GAB1-SHP2 PLA signals were colocalized with EGFR. This observation is consistent with our previous observations from cell fractionation experiments that GAB1-SHP2 complexes are primarily cytosolic and that GAB1-SHP2 association with EGFR also decreases over time in HeLa cells (*12*). Additionally, GAB1-SHP2 PLA signals can be seen both proximal

to the cell membrane (mV-HRAS signal) and throughout the cell interior. Thus, the PLA results provide experimental support for our model that GAB1-SHP2 complexes can exist separately from the signal-initiating EGFR and throughout the cytosol in response to EGF.

DISCUSSION

The predictions of our reaction-diffusion model suggest that membrane-bound EGFR regulates signaling over the entire intracellular length scale through GAB1-SHP2 complexes that are maintained by the intermediary action of SFKs (Fig. 8). This conceptual model stands in contrast to the more conventional view that receptor-bound complexes, such as GAB1-SHP2, access different subcellular compartments through directed membrane localization and trafficking processes. This new understanding may help explain prior apparently contradictory observations. For example, recent work demonstrates that RAS activity and ERK phosphorylation paradoxically remain dependent on EGFR activity even after EGFR and RAS become physically separated due to EGFR endocytosis and membrane retention of RAS (*40, 45, 52*). Based on our work, GAB1-SHP2 complexes, generated by active endocytosed EGFR, may diffuse back to the cell membrane and thereby promote RAS activity. SHP2 promotes RAS activity via dephosphorylation of GAB1 at Y317, a p120-RASGAP (RASA1) binding site (*13*), or by dephosphorylating RASGAP binding sites directly on EGFR. Other mechanisms of RAS regulation by SHP2 have been proposed (*6, 53-55*), including the possibility of SHP2 acting as a scaffold that recruits GRB2-SOS complexes to the cell membrane (*7, 56*). Aside from regulating RAS activity, SHP2 has also been reported to regulate the phosphorylation of paxillin (*57, 58*) and the transmembrane adaptor protein PAG/CBP (*53*). Thus, there are several SHP2 signaling targets that our analysis suggests EGFR can distally regulate via the reaction-diffusion mechanism described here.

Our analysis reveals that GAB1-SHP2 complex maintenance throughout the cytosol is promoted by SFK phosphorylation of GAB1 tyrosines. Interestingly, a prior study noted impaired EGF-mediated SRC Y418 phosphorylation in the non-small cell lung cancer (NSCLC) cell line H3255, which expresses a kinase-activated EGFR mutant that confers sensitivity to EGFR

inhibition (*59*). H3255 cells also have a functional impairment in EGFR-mediated SHP2 activity and inability to drive ERK activity as efficiently as NSCLC cells expressing wild-type EGFR (*60*). Thus, EGFR may rely heavily on SFKs to activate ERK through SHP2, and disruption of this mechanism may occur with certain EGFR mutations that render cells susceptible to EGFR inhibitors.

Our analysis indicates that the GAB1-SHP2 persistence length scale is sensitive to perturbations in the rate constants for GAB1-SHP2 association and dissociation, SFK inactivation, and GAB1 dephosphorylation, but is surprisingly much less sensitive to the rate constants for SFK activation and GAB1 phosphorylation (Fig. 3A). In fact, the rate constant for SFK activation had essentially no control over the steady state cellular distribution of GAB1-SHP2 complexes. This is likely the result of a model topology wherein SFKs are activated only at the cell surface by membrane-bound EGFR. SFKs will be rapidly inactivated throughout the cytosol even if SFK activation is made more rapid. The appearance of the rate constant for SFK inactivation but not activation in our order-of-magnitude estimate for active SFKs (Eq. [13]) is consistent with this understanding. This view of the system is also consistent with our finding that EGFR only weakly controls the spatial gradient of GAB1-SHP2 complexes within the cell (Fig. 3A).

Characteristic time scales for the reaction-diffusion mechanism modeled here suggest that GAB1 may require phosphorylation up to 3-4 times by SFKs throughout the cytosol to permit an individual GAB1-SHP2 complex to diffuse to the cell center from the cell surface, but the time scale of SFK inactivation suggests that GAB1 can only be phosphorylated once before SFKs become inactivated. The time scales for SHP2 binding and unbinding from GAB1, however, are much smaller than the time scale for GAB1 dephosphorylation. For a pGAB1 molecule to diffuse to the cell center, at least 6-7 SHP2 binding events may occur prior to GAB1 dephosphorylation.

This is reflected in the strong predicted sensitivity of GAB1-SHP2 persistence and abundance to changes in SHP2 expression and GAB1-SHP2 binding kinetics. Thus, even with active SFKs primarily localized near the cell membrane, protective SHP2 binding to pGAB1 promotes the maintenance of GAB1-SHP2 complexes away from the cell surface.

The future refinement and verification of the model developed here would be greatly aided by time-resolved measurements of the distribution of GAB1-SHP2 complexes within a cell, such as could be obtained from live-cell FRET microscopy. While a GAB1-SHP2 FRET reporter pair is not presently available, our PLA experiments (Fig. 7) and previous findings using cell fractionation (*12*) show that GAB1-SHP2 complexes exist primarily in the cytosol rather than membrane compartments. PLA experiments capture only snapshots of protein-protein interactions from fixed cells and may not fully capture all reversible protein-protein binding events occurring within cells. Model calculations with HeLa abundances predict that ~300-400 GAB1-SHP2 molecules are formed per cell in response to EGF treatment, which is about an order of magnitude greater than the amount measured by PLA. Live-cell FRET experiments may more accurately capture the dynamics and spatial distribution of GAB1-SHP2 association in cells. It would also be beneficial to measure the diffusivity of all the cytosolic proteins in the model (e.g., by fluorescence recovery after photobleaching), as our current predictions rely on using empirical relationships to estimate diffusivities based on protein and complex molecular weights (*35, 36*). In addition to refining model parameters, additional cellular processes can be incorporated into the model to more completely describe the steps leading to cytosolic protein complex assembly, including receptor endocytosis (*61-63*) and coordinated protein complex assembly via cytosolic scaffold proteins (*64*). Given that RTKs including EGFR and TrkA can nucleate signaling complex formation from endosomes (*61-63, 65*), consideration of these processes in future spatial models

will be important for more completely understanding the ability of receptors to regulate signaling events at a distance via reaction-diffusion mechanisms such as the one described here.

Mechanisms similar to that described for EGFR may exist for other receptors, including other ErbB receptor family members, capable of activating diffusible non-receptor kinases that phosphorylate protein complex constituents. ErbB2/HER2, for example, activates SFKs (*66*) and promotes GAB1 phosphorylation and association with SHP2 (*67*). SHP2 is also required for complete activation of ERK and other pathways downstream of MET and fibroblast growth factor receptors (FGFRs) (*17, 68, 69*), but the spatiotemporal regulation of SHP2 activity differs between these receptor systems and compared to EGFR. In some cell contexts, MET may drive lower but more sustained and membrane-localized GAB1-SHP2 association (*12, 18*). In response to FGFR activation, SHP2 binds preferentially to the membrane-bound adaptor FRS2 (*70*). These observations highlight the possibility that different receptors induce SHP2 activity with different dynamics and subcellular localization of GAB1-SHP2, and that not all receptors may be capable of regulating signaling over the entire cytosolic domain via GAB1-SHP2 complexes. We hypothesize that endocytosed EGFR, for example, may continue to regulate RAS signaling at the membrane via diffusible GAB1-SHP2, but such a mechanism may not exist or be necessary for other receptors, particularly if the trafficking dynamics of those receptors differ substantially from EGFR. Computational modeling is an invaluable tool in investigating such hypotheses, and our model provides a platform upon which future models could be built to study the spatiotemporal regulation of cytosolic phospho-proteins or protein complexes initiated by the activity of membrane-associated receptors and RTKs.

ACKNOWLEDGEMENTS

This work was supported by the National Science Foundation 1716537 (MJL), the University of Virginia Biomedical Data Sciences Training Program NIH T32 LM012416, University of Pennsylvania Training Program in Cancer Pharmacology (R25 CA101871), and the Ashton Foundation. The Virtual Cell is supported by NIH Grant Number P41 GM103313 from the National Institute for General Medical Sciences.

Figures

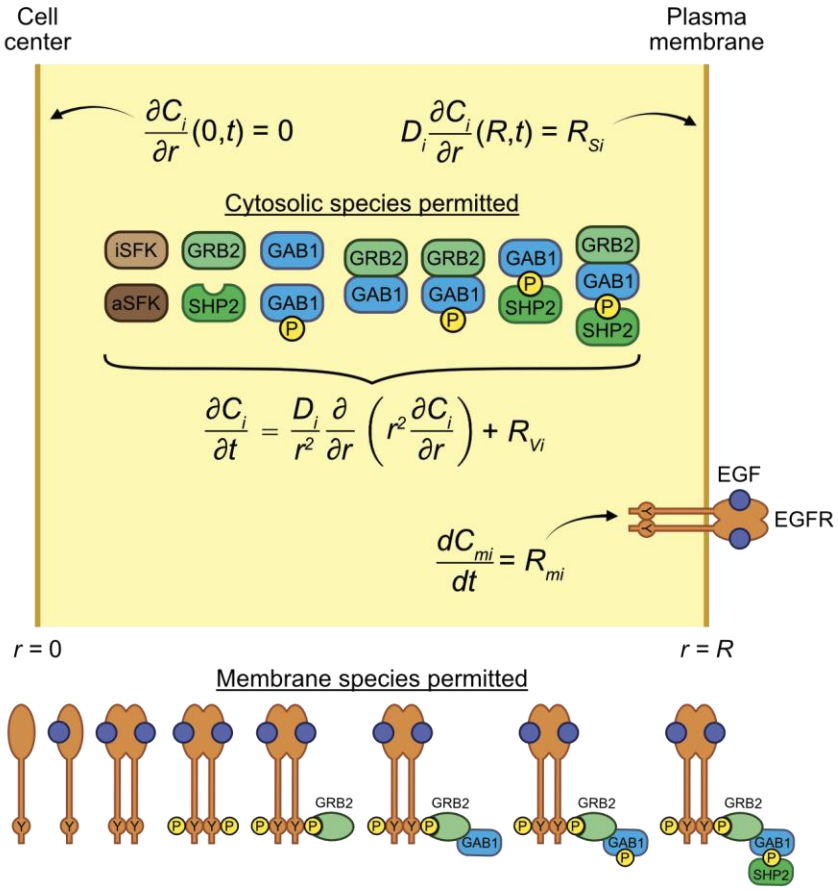

Fig. 1. Model schematic. The cell cytosolic compartment is modeled as a sphere of radius R = 10 μm. The dependence of protein and protein complex concentrations on position and time after EGFR activation was modeled using standard reaction-diffusion equations. No-flux boundary conditions were imposed at the cell center consistent with symmetry of the problem, and Robin boundary conditions were imposed at the cell membrane to reflect the equivalence between reaction and diffusion of species at $r = R$. Membrane-bound species were assumed to be homogenously distributed in that compartment and were therefore modeled only as a function of time.

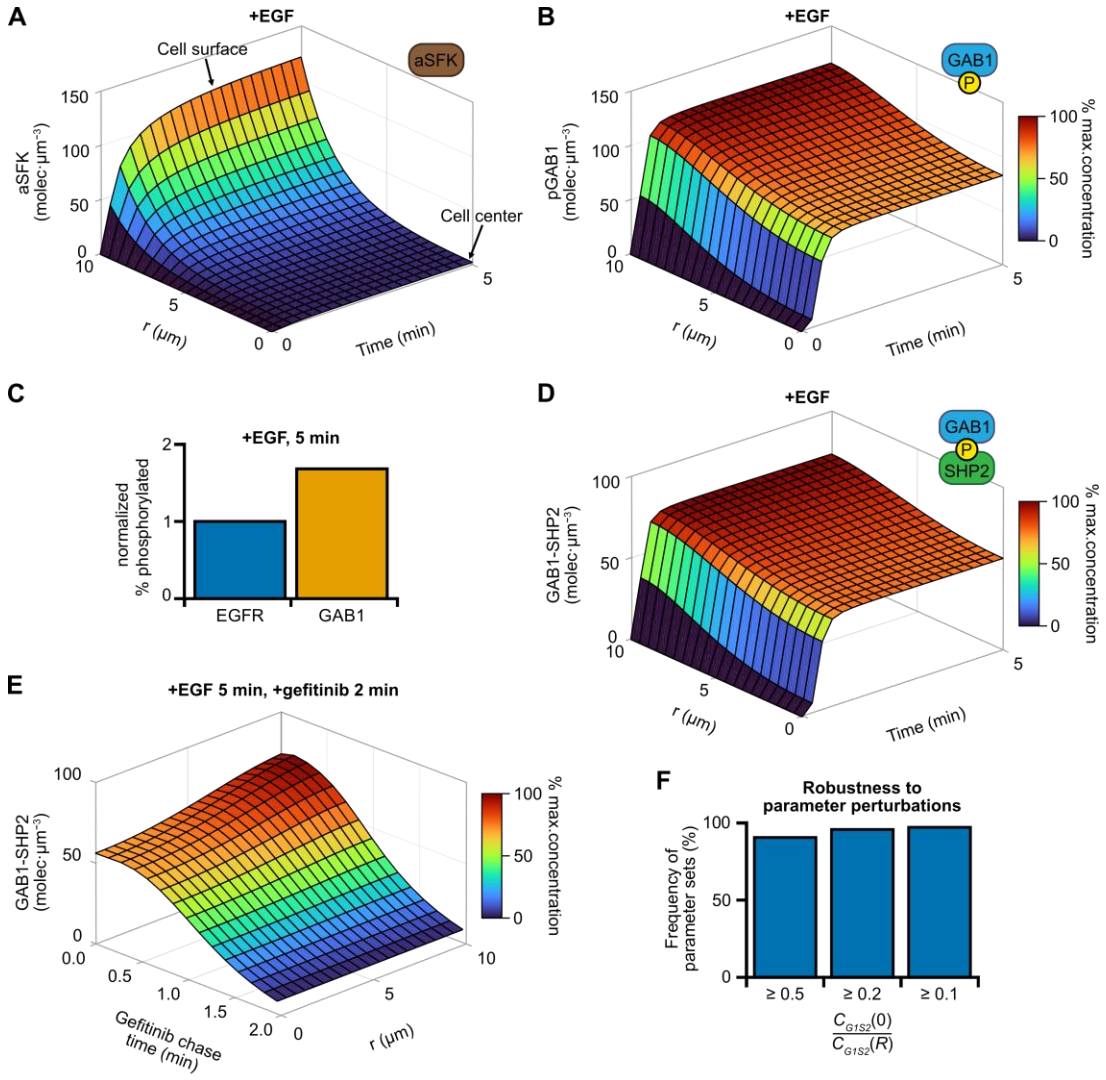

Fig. 2. GAB1-SHP2 complexes are well distributed throughout cells in response to EGFR activation. (**A-B**) For the base parameters, model predictions are shown for the concentrations of active SFKs and phosphorylated GAB1 in response to 10 ng/mL EGF as a function of distance from the cell center (*r*) and time. (**C**) Average concentrations of phosphorylated EGFR and GAB1 in response to 10 ng/mL EGF at t = 5 min were computed and normalized to the average concentration of phosphorylated EGFR. (**D**) Model predictions for the concentration of GABl-SHP2 complexes as a function of *r* and time are shown. (**E**) The concentration of GAB1-SHP2 complexes was predicted as a function of *r* and time for an initial 5-min pulse of 10 ng/mL EGF chased by a 2-min treatment with the EGFR inhibitor gefitinib. Gefitinib treatment was simulated by setting the rate constant for EGFR phosphorylation to 0. Model predictions are shown for the 2-min chase time course. (**F**) Model predictions were made for 1,000 parameter sets in which each parameter was randomly varied by up to a factor of 10 above or below its base value. Robustness of the model length scale predictions was assessed by calculating the percentage of simulations in which the ratio of GAB1-SHP2 concentrations at the cell center to the cell surface

($C_{G1S2}(0)/C_{G1S2}(R)$) was ≥ 0.5, 0.2, and 0.1. Protein diffusivities were collectively perturbed by the same factor in these simulations.

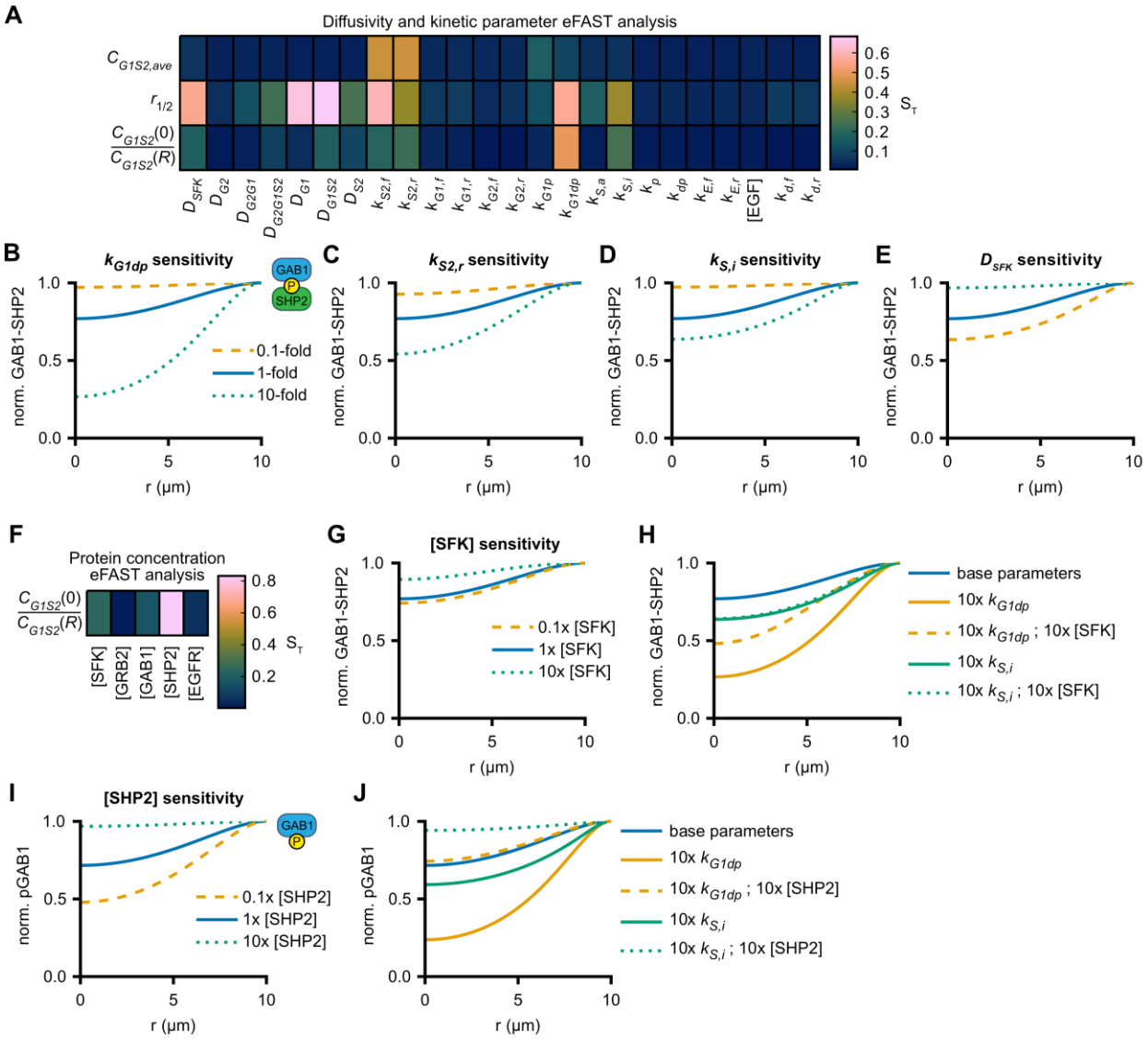

Fig. 3. Model sensitivity analysis identifies processes controlling the length scale of GAB1-SHP2 persistence. (**A**) Extended Fourier amplitude sensitivity test (eFAST) was used to perform parameter sensitivity analysis of model predictions for the spatially averaged concentration of GAB1-SHP2 complexes ($C_{G1S2,ave}$), the distance over which the GAB1-SHP2 concentration decays to 1/2 of the maximum GAB1-SHP2 concentration at the cell surface ($r_{1/2}$), and the ratio of GAB1-SHP2 concentrations at the cell center to the cell surface ($C_{G1S2}(0)$/ $C_{G1S2}(R)$) after a 5-min EGF treatment (10 ng/mL). Model sensitivities were calculated as total-order eFAST indices (S_T) where model parameters were permitted to vary by up to a factor of 10 above or below their base values over 24,000 simulations (1,000 simulations per parameter varied). (**B-E**) Model predictions for the normalized concentration of GAB1-SHP2 after a 5-min EGF treatment (10 ng/mL) were compared with predictions when k_{G1dp}, $k_{S2,r}$, $k_{S,i}$, or D_{SFK} were varied by a factor of 10 as indicated. (**F**) eFAST was used to assess the model sensitivity to changes in initial protein concentrations when allowing the abundance of each protein to vary between 100 and 1,000,000 molecules per cell over 5,000 total simulations. (**G-H**) Model predictions for the normalized concentration of GAB1-SHP2 or

pGAB1 after 5-min EGF treatment were compared with predictions when the concentration of SFKs or the indicated kinetic parameters were varied by a factor of 10 as indicated. (**I-J**) Model predictions for the normalized concentration of phosphorylated GAB1 after a 5-min EGF treatment (10 ng/mL) were compared with predictions when the concentration of SHP2 or the indicated kinetic parameters were varied by a factor of 10 as indicated. In panels (B-E) and (G-J), the concentration of GAB1-SHP2 was normalized to the maximum value within each individual curve.

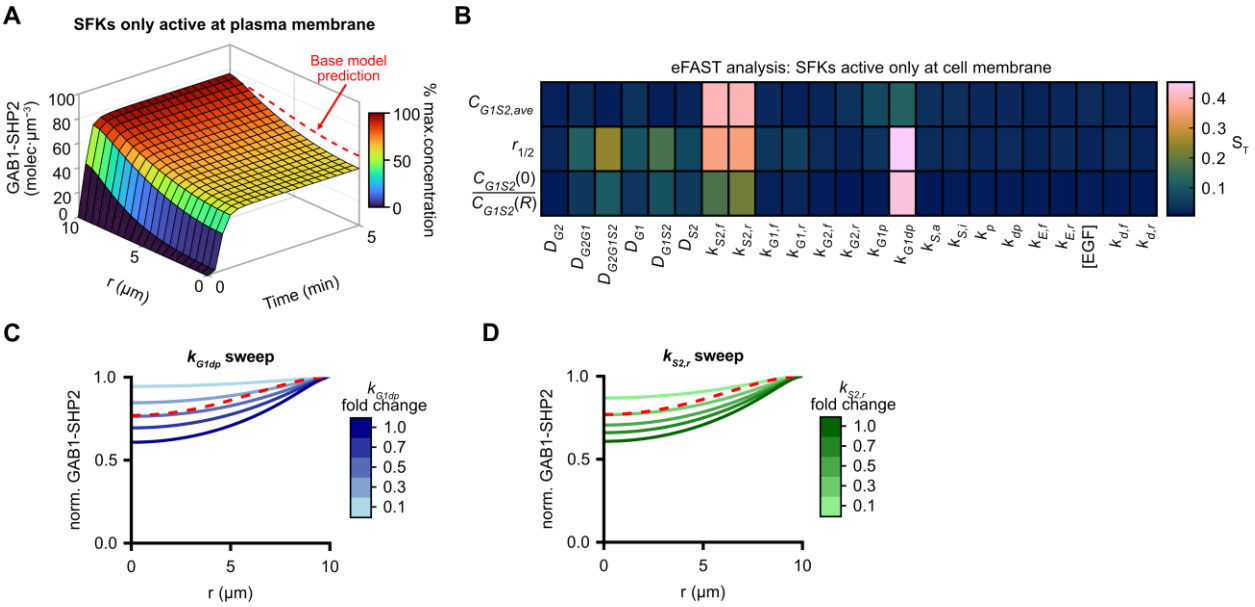

Fig. 4. Confining SFK activity to the plasma membrane modestly reduces GAB1-SHP2 complex persistence. (**A**) Model predictions for the concentrations GAB1-SHP2 complexes were plotted as a function of distance from the cell center (*r*) and time following 10 ng/mL EGF treatment when SFKs were only permitted to be active at the cell surface for the base model parameters. (**B**) eFAST was used to perform parameter sensitivity analysis of $C_{G1S2,ave}$, $r_{1/2}$, and $C_{G1S2}(0)/ C_{G1S2}(R)$ after a 5-min 10 ng/mL EGF treatment when active SFKs were confined to the plasma membrane. Model sensitivities were calculated as total-order eFAST indices (S_T) where model parameters were permitted to vary by up to a factor of 10 above or below their base values (1,000 simulations per parameter varied). (**C**, **D**) Model predictions are shown for the normalized concentration of GAB1-SHP2 after a 5-min 10 ng/mL EGF treatment when active SFKs were confined to the plasma membrane and where k_{G1dp} and $k_{S2,r}$ were varied by the indicated fold changes from their base values. The concentration of GAB1-SHP2 was normalized to the maximum value within each curve. For comparison, the baseline model prediction for normalized or unnormalized GAB1-SHP2 concentration profile at t = 5 min (with diffusible active SFKs) is shown as a dashed red line in all panels except (B).

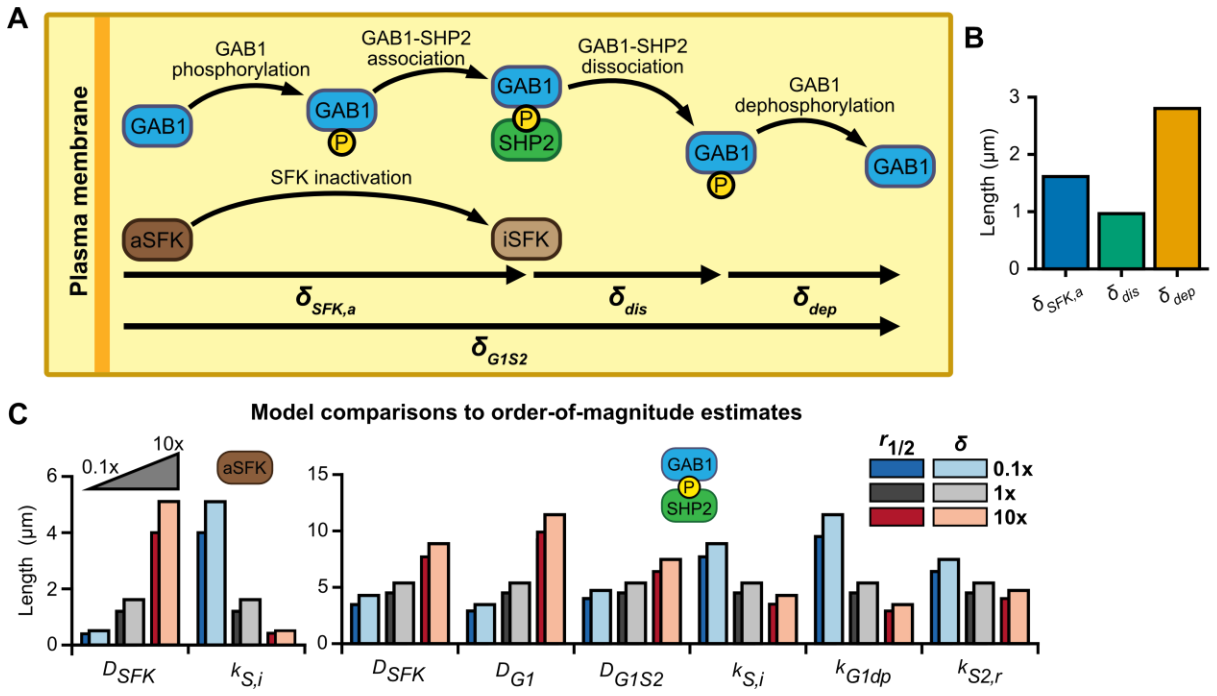

Fig. 5. Order of magnitude length scale estimates support the conclusions of the full model. (**A**) The key reaction-diffusion processes used to estimate an order-of-magnitude length scale estimate for GAB1-SHP2 association are illustrated schematically. Over the length scale for which SFKs are active ($\delta_{SFK,a}$), GAB1 is phosphorylated, which enables its binding to SHP2. Beyond the length scale over which SFKs remain active distal from EGFR, GAB1-SHP2 association is extended by the length scales over which GAB1-SHP2 dissociates (δ_{dis}) and GAB1 dephosphorylation occurs (δ_{dep}). (**B**) Estimates for $\delta_{SFK,a}$, δ_{dis}, and δ_{dep} were calculated using the base model parameters from Table 1. (**C**) Model predictions for the distance over which the concentrations of active SFKs and GAB1-SHP2 fall to half their concentrations at the cell surface ($r_{1/2}$) were compared to order-of-magnitude estimates for the length scales (δ) over which these species persist distal from the cell surface when the indicated parameters were varied by a factor of 10 from their base values. Model predictions for $r_{1/2}$ were made by setting the cell radius to 50 μm because length scale values > 10 μm could not be obtained with the base cell radius of 10 μm. In (C), $r_{1/2}$ is denoted by darker bars shifted slightly to the left; δ values were calculated according to Eqs. 13 and 16 and are denoted by lighter, right-shifted bars.

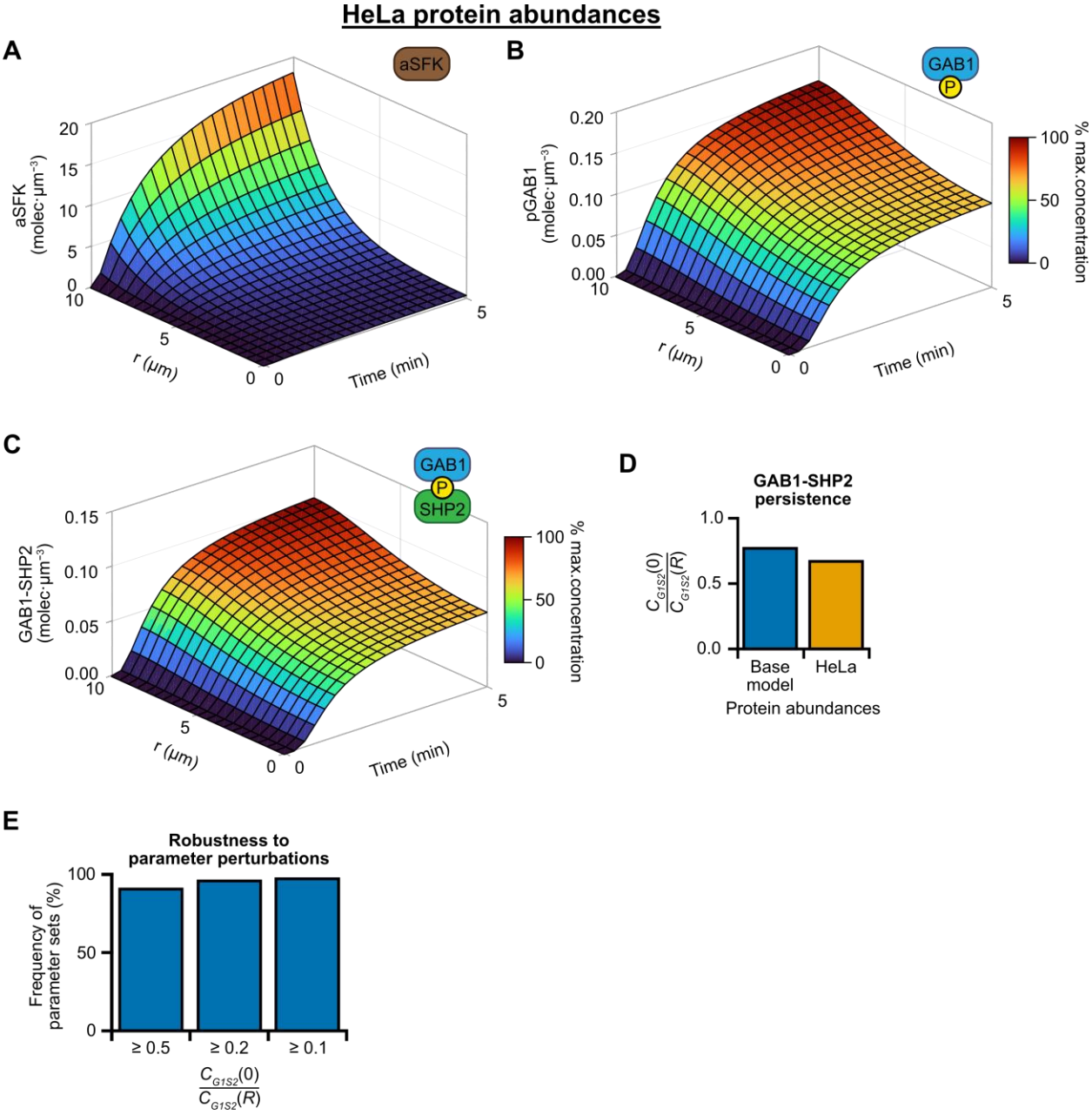

Fig. 6. Qualitative model predictions hold for HeLa cell protein abundances, which include a stoichiometrically limiting concentration of GAB1. (**A-C**) Model predictions using HeLa protein abundances for the concentrations of active SFKs, phosphorylated GAB1, and GAB1-SHP2 complexes were plotted as a function of distance from the cell center (r) and time following a 5-min 10 ng/mL EGF treatment. (**D**) Model predictions for $C_{G1S2}(0)/C_{G1S2}(R)$ were calculated for a 5-min EGF treatment (10 ng/mL) when using the base model protein abundances and HeLa protein abundances. (**E**) Using HeLa protein abundances, model predictions were calculated for 1,000 parameter sets in which each parameter was randomly varied by up to a factor of 10 above or below its base value. Robustness of the model length scale predictions was then assessed by calculating the percentage of simulations in which $C_{G1S2}(0)/C_{G1S2}(R)$ was $\geq$ to 0.5, 0.2, and 0.1. Protein diffusivities were collectively perturbed by the same factor in these simulations.

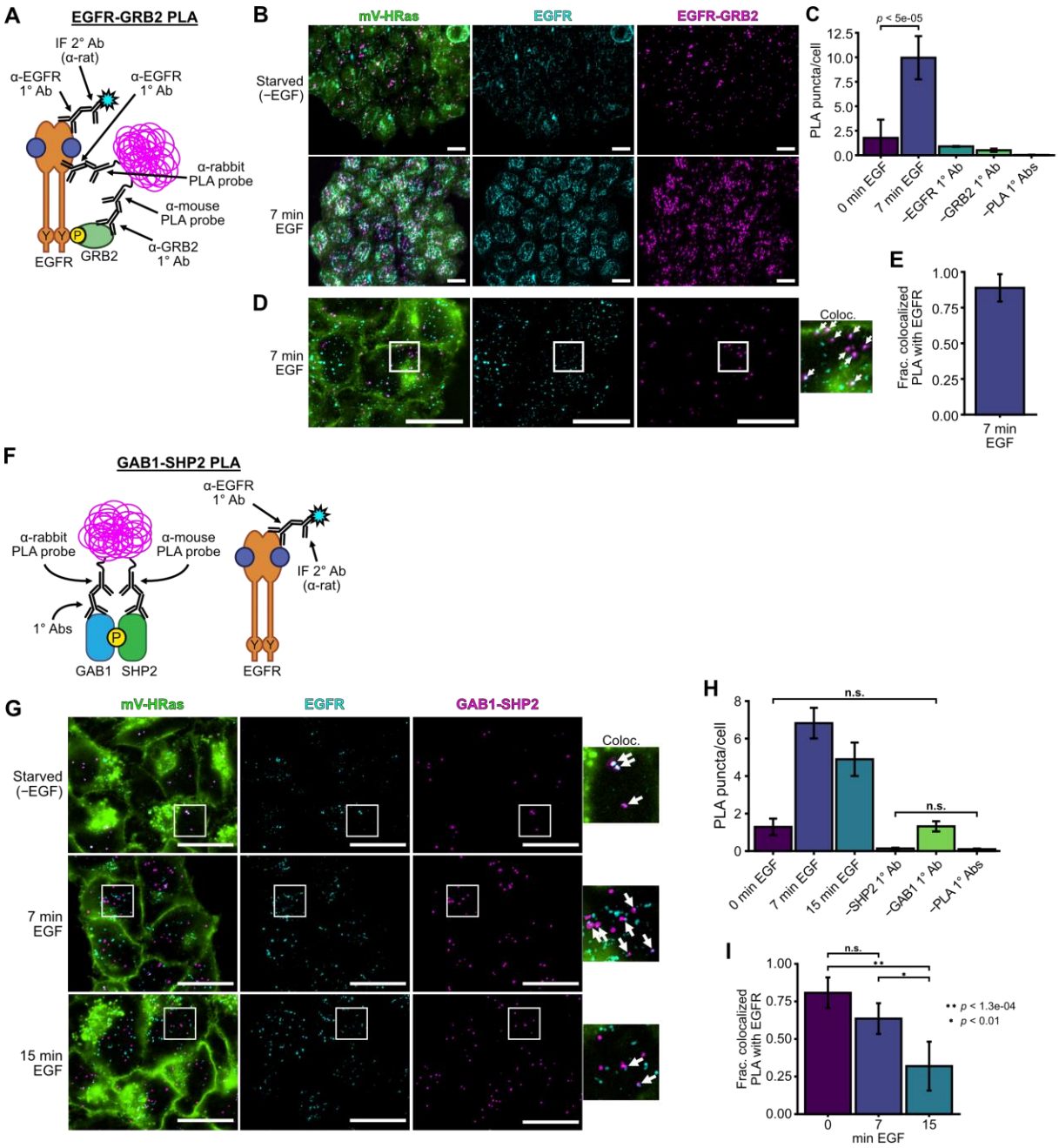

Fig. 7. GAB1-SHP2 complexes are distributed throughout the cytoplasm and distal from EGFR in EGF-treated cancer cells. (**A**) Schematic representation of the proximity ligation assay (PLA) and experimental setup. EGFR-GRB2 complexes were stained via PLA and EGFR was stained via standard immunofluorescence (IF) using an alternative EGFR antibody to confirm the colocalization of the two signals. (**B**) Images of HeLa/mVenus-HRAS that were treated with 10 ng/mL EGF as indicated, fixed, and stained for EGFR and EGFR-GRB2 by IF and PLA, respectively. Scale bars, 20 μm. (**C**) Quantification of PLA signals per cell for the conditions shown in (B) and PLA primary antibody controls (Fig. S4A) were computed. Welch's ANOVA indicated a statistically significant difference among groups ($F = 247.86$, $p < 1.363\times10^{-8}$), and the Games-Howell post-hoc test was used to determine *p* values for pairwise comparisons. (**D**) High-

magnification images of HeLa/mV-HRAS cells treated as indicated and stained via IF and PLA for EGFR and EGFR-GRB2, respectively. The far-right panel ("Coloc.") shows 2.5× magnification of the region marked by the white square. White arrows indicate colocalization between EGFR and EGFR-GRB2 puncta. (**E**) Fraction of EGFR-GRB2 PLA puncta co-localized with EGFR puncta in treated HeLa/mV-HRAS cells stained using the full PLA reaction for the images shown in (D). Error bars, 95% confidence intervals. Scale bars, 20 μm. Images are representative of N = 3 to 5 independent coverslips per condition. (**F**) A combination of proximity ligation assay (PLA) for GAB1 and SHP2 and standard immunofluorescence (IF) for EGFR was used to determine the localization of GAB1-SHP2 complexes relative to EGFR. The schematic shows the basic elements of the approach for using three primary and three secondary antibodies. (**G**) HeLa cells expressing mVenus-HRAS were treated with 10 ng/mL EGF for $t \leq 15$ min, fixed, and stained for PLA and IF. Maximum-intensity *z*-projections from epifluorescence imaging are shown. The rightmost column ("colocalization") shows 2.5× magnifications of the regions indicated by white rectangles. White arrows indicate colocalization (overlap) of EGFR and GAB1-SHP2 signals (i.e., EGFR and GAB1-SHP2 colocalization). Scale bars, 20 μm. Images are representative of n = 5 to 10 independent coverslips per condition. (**H**) PLA puncta per cell for conditions in (G) and PLA primary antibody controls (Fig. S4B) were computed. Welch's ANOVA indicated a statistically significant difference among groups ($F = 90.876$, $p < 2.2 \times 10^{-16}$). The Games-Howell post hoc test was used to determine between-group significance. $p < 0.05$ except for the two comparisons indicated. (**I**) The fraction of GAB1-SHP2 puncta co-localized with EGFR puncta was computed. Welch's ANOVA indicated the presence of statistically significant differences among groups ($F = 12.153$, $p < 1.5 \times 10^{-4}$), and Games-Howell post-hoc test was used to compute the *p* values shown. Error bars in C and D, 95% confidence intervals.

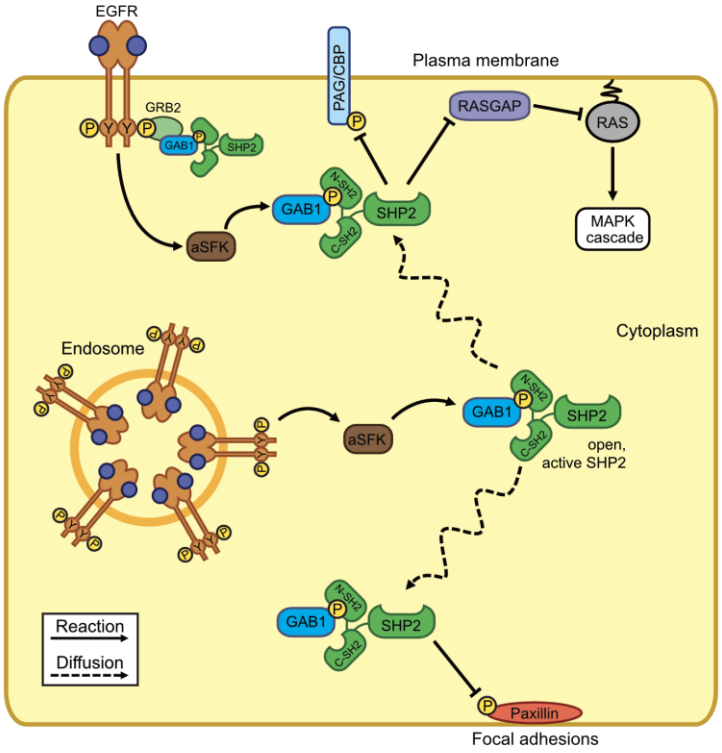

Fig. 8. Diffusible GAB1-SHP2 complexes enable EGFR to regulate signaling processes distal from the receptor. Through the intermediate action of SFKs, EGFR promotes the formation of GAB1-SHP2 complexes, and hence active SHP2, which can then diffuse to different cellular locations and act on substrates involved in signaling pathways and cytoskeletal regulation. In cell backgrounds where the majority of EGFR is rapidly internalized after receptor activation, EGFR may still be able to influence signaling processes at the plasma membrane and in other cellular compartments via the activation of diffusible signaling complexes such as GAB1-SHP2.

Table 1. Model parameters

Parameter (units)	Description	Value	Source
$k_{E,f}$ (μM^{-1} min^{-1})	EGF binding to EGFR, forward	3.1×10^{2}	(*29*)
$k_{E,r}$ (min^{-1})	EGF binding to EGFR, reverse	8.0×10^{-1}	(*30*)
$k_{dE,f}$ (μm^2 $molec^{-1}$ min^{-1})	EGFR dimerization, forward	1.2×10^{0}	(*12*)
$k_{dE,r}$ (min^{-1})	EGFR dimerization, reverse	1.0×10^{-1}	(*71*)
k_{catE} (min^{-1})	EGFR phosphorylation, EGF-occupied dimer	1.3×10^{1}	(*72*)
k_{dp} (min^{-1})	EGFR dephosphorylation	8.0×10^{0}	(*12*)
$k_{S,a}$ (μm^3 $molec^{-1}$ min^{-1})	SFK activation	7.7×10^{-1}	Fit
$k_{S,i}$ (min^{-1})	SFK inactivation	3.2×10^{1}	Fit
$k_{G2,f}$ (μm^3 $molec^{-1}$ min^{-1})	GRB2 binding to EGFR, forward	1.6×10^{0}	(*2*)
$k_{G2,r}$ (min^{-1})	GRB2 binding to EGFR, reverse	4.6×10^{2}	(*2*)
$k_{G1,f}$ (μm^3 $molec^{-1}$ min^{-1})	GAB1 binding to GRB2, forward	1.0×10^{-1}	(*73*)
$k_{G1,r}$ (min^{-1})	GAB1 binding to GRB2, reverse	6.0×10^{1}	(*73*)
k_{G1p} (μm^3 $molec^{-1}$ min^{-1})	GAB1 phosphorylation	2.7×10^{-1}	Fit
k_{G1dp} (min^{-1})	GAB1 dephosphorylation	8.4×10^{0}	Fit
$k_{S2,f}$ (μm^3 $molec^{-1}$ min^{-1})	SHP2 binding to phosphorylated GAB1, forward	1.6×10^{0}	(*74*)
$k_{S2,r}$ (min^{-1})	SHP2 binding to phosphorylated GAB1, reverse	4.6×10^{2}	(*74*)
$C_{o,EGF}$ (μM)	Extracellular EGF concentration	1.7×10^{-3}	See text
$C_{o,EGFR}$ ($cell^{-1}$)	EGFR molecules per cell	6.0×10^{5}	(*12*)
$C_{o,GRB2}$ ($cell^{-1}$)	GRB2 molecules per cell	6.0×10^{5}	(*73*)
$C_{o,GAB1}$ ($cell^{-1}$)	GAB1 molecules per cell	6.0×10^{5}	(*73*)
$C_{o,SHP2}$ ($cell^{-1}$)	SHP2 molecules per cell	6.0×10^{5}	(*73*)
$C_{o,SFK}$ ($cell^{-1}$)	SFK molecules per cell	6.0×10^{5}	(*73*)
D_{SFK} (μm^2 min^{-1})	Diffusivity of SFK molecules	8.2×10^{1}	(*35*, *36*)
D_{G2} (μm^2 min^{-1})	Diffusivity of GRB2 molecules	1.3×10^{2}	(*35*, *36*)
D_{G2G1} (μm^2 min^{-1})	Diffusivity of GRB2-GAB1 molecules	6.1×10^{1}	(*35*, *36*)
D_{G2G1S2} (μm^2 min^{-1})	Diffusivity of GRB2-GAB1-SHP2 molecules	5.5×10^{1}	(*35*, *36*)
D_{G1} (μm^2 min^{-1})	Diffusivity of GAB1 molecules	6.6×10^{1}	(*35*, *36*)
D_{G1S2} (μm^2 min^{-1})	Diffusivity of GAB1-SHP2 molecules	5.6×10^{1}	(*35*, *36*)
D_{S2} (μm^2 min^{-1})	Diffusivity of SHP2 molecules	7.8×10^{1}	(*35*, *36*)
R (μm)	Cell radius	1.0×10^{1}	(*28*)

REFERENCES

1. B. J. Mayer, Perspective: Dynamics of receptor tyrosine kinase signaling complexes. *FEBS Lett* **586**, 2575-2579 (2012).
2. M. Morimatsu *et al.*, Multiple-state reactions between the epidermal growth factor receotor and Grb2 as observed by using single-molecule analysis. *P Natl Acad Sci USA* **104**, 18013-18018 (2007).
3. M. M. Zhou *et al.*, Binding affinities of tyrosine-phosphorylated peptides to the COOH-terminal SH2 and NH2-terminal phosphotyrosine binding domains of Shc. *J Biol Chem* **270**, 31119-31123 (1995).
4. M. Offterdinger, V. Georget, A. Girod, P. I. H. Bastiaens, Imaging phosphorylation dynamics of the epidermal growth factor receptor. *J Biol Chem* **279**, 36972-36981 (2004).
5. A. Sorkin, M. McClure, F. T. Huang, R. Carter, Interaction of EGF receptor and Grb2 in living cells visualized by fluorescence resonance energy transfer (FRET) microscopy. *Curr Biol* **10**, 1395-1398 (2000).
6. T. A. Ahmed *et al.*, SHP2 Drives Adaptive Resistance to ERK Signaling Inhibition in Molecularly Defined Subsets of ERK-Dependent Tumors. *Cell Rep* **26**, 65-+ (2019).
7. K. S. Grossmann, M. Rosario, C. Birchmeier, W. Birchmeier, The Tyrosine Phosphatase Shp2 in Development and Cancer. *Adv Cancer Res* **106**, 53-89 (2010).
8. M. Dance, The molecular functions of Shp2 in the Ras/Mitogen-activated protein kinase (ERK1/2) pathway. *Cell Signal* **20**, 453-459.
9. B. G. Neel, H. H. Gu, L. Pao, The 'Shp'ing news: SH2 domain-containing tyrosine phosphatases in cell signaling. *Trends Biochem Sci* **28**, 284-293 (2003).
10. H. H. Gu, B. G. Neel, The 'Gab' in signal transduction. *Trends Cell Biol* **13**, 122-130 (2003).
11. H. Daub, C. Wallasch, A. Lankenau, A. Herrlich, A. Ullrich, Signal characteristics of G protein-transactivated EGF receptor. *Embo J* **16**, 7032-7044 (1997).
12. C. M. Furcht, J. M. Buonato, M. J. Lazzara, EGFR-activated Src family kinases maintain GAB1-SHP2 complexes distal from EGFR. *Science Signaling* **8**, (2015).
13. A. Montagner *et al.*, A novel role for Gab1 and SHP2 in epidermal growth factor-induced ras activation. *J Biol Chem* **280**, 5350-5360 (2005).
14. G. A. Rodrigues, M. Falasca, Z. T. Zhang, S. H. Ong, J. Schlessinger, A novel positive feedback loop mediated by the docking protein Gab1 and phosphatidylinositol 3-kinase in epidermal growth factor receptor signaling. *Mol Cell Biol* **20**, 1448-1459 (2000).
15. M. Incoronato *et al.*, The Shp-1 and Shp-2, tyrosine phosphatases, are recruited on cell membrane in two distinct molecular complexes including Ret oncogenes. *Cell Signal* **16**, 847-856 (2004).
16. X. D. Zhou, Y. M. Agazie, Molecular Mechanism for SHP2 in Promoting HER2-induced Signaling and Transformation. *J Biol Chem* **284**, 12226-12234 (2009).
17. U. Schaeper *et al.*, Coupling of Gab1 to c-Met, Grb2, and Shp2 mediates biological responses. *J Cell Biol* **149**, 1419-1432 (2000).
18. C. R. Maroun, M. A. Naujokas, M. Park, Membrane targeting of Grb2-associated binder-1 (Gab1) scaffolding protein through src myristoylation sequence substitutes for Gab1 pleckstrin homology domain and switches an epidermal growth factor response to an invasive morphogenic program. *Mol Biol Cell* **14**, 1691-1708 (2003).

19. C. L. Abram, S. A. Courtneidge, Src family tyrosine kinases and growth factor signaling. *Exp Cell Res* **254**, 1-13 (2000).
20. K. V. Lu *et al.*, Fyn and Src Are Effectors of Oncogenic Epidermal Growth Factor Receptor Signaling in Glioblastoma Patients. *Cancer Res* **69**, 6889-6898 (2009).
21. N. Osherov, A. Levitzki, Epidermal-Growth-Factor-Dependent Activation of the Src-Family Kinases. *Eur J Biochem* **225**, 1047-1053 (1994).
22. P. A. Bromann, H. Korkaya, S. A. Courtneidge, The interplay between Src family kinases and receptor tyrosine kinases. *Oncogene* **23**, 7957-7968 (2004).
23. M. C. Maa, T. H. Leu, D. J. McCarley, R. C. Schatzman, S. J. Parsons, Potentiation of epidermal growth factor receptor-mediated oncogenesis by c-Src: implications for the etiology of multiple human cancers. *Proceedings of the National Academy of Sciences* **92**, 6981-6985 (1995).
24. M. Okada, H. Nakagawa, A Protein Tyrosine Kinase Involved in Regulation of Pp60c-Src Function. *J Biol Chem* **264**, 20886-20893 (1989).
25. L. K. Bieniasz, The von Neumann stability of finite-difference algorithms for the electrochemical kinetic simulation of diffusion coupled with homogeneous reactions. *Journal of Electroanalytical Chemistry* **345**, 13-25 (1993).
26. D. C. Resasco *et al.*, Virtual Cell: computational tools for modeling in cell biology. *Wires Syst Biol Med* **4**, 129-140 (2012).
27. M. L. Blinov *et al.*, Compartmental and Spatial Rule-Based Modeling with Virtual Cell. *Biophys J* **113**, 1365-1372 (2017).
28. B. N. Kholodenko, MAP kinase cascade signaling and endocytic trafficking: a marriage of convenience? *Trends Cell Biol* **12**, 173-177 (2002).
29. C. M. Waters, K. C. Oberg, G. Carpenter, K. A. Overholser, Rate Constants for Binding, Dissociation, and Internalization of Egf - Effect of Receptor Occupancy and Ligand Concentration. *Biochemistry-Us* **29**, 3563-3569 (1990).
30. A. R. French, D. K. Tadaki, S. K. Niyogi, D. A. Lauffenburger, Intracellular Trafficking of Epidermal Growth-Factor Family Ligands Is Directly Influenced by the Ph Sensitivity of the Receptor-Ligand Interaction. *J Biol Chem* **270**, 4334-4340 (1995).
31. Y. B. Shan *et al.*, Oncogenic Mutations Counteract Intrinsic Disorder in the EGFR Kinase and Promote Receptor Dimerization. *Cell* **149**, 860-870 (2012).
32. N. Borisov *et al.*, Systems-level interactions between insulin–EGF networks amplify mitogenic signaling. *Molecular Systems Biology* **5**, 256 (2009).
33. J. S. Biscardi *et al.*, c-Src-mediated phosphorylation of the epidermal growth factor receptor on Tyr845 and Tyr1101 is associated with modulation of receptor function. *J Biol Chem* **274**, 8335-8343 (1999).
34. R. Roskoski, Jr., Src protein-tyrosine kinase structure, mechanism, and small molecule inhibitors. *Pharmacol Res* **94**, 9-25 (2015).
35. R. Pepperkok, M. H. Bre, J. Davoust, T. E. Kreis, Microtubules are stabilized in confluent epithelial cells but not in fibroblasts. *J Cell Biol* **111**, 3003-3012 (1990).
36. H. P. Erickson, Size and Shape of Protein Molecules at the Nanometer Level Determined by Sedimentation, Gel Filtration, and Electron Microscopy. *Biol Proced Online* **11**, 32-51 (2009).
37. S. Marino, I. B. Hogue, C. J. Ray, D. E. Kirschner, A methodology for performing global uncertainty and sensitivity analysis in systems biology. *J Theor Biol* **254**, 178-196 (2008).

38. A. Saltelli, S. Tarantola, K. P. S. Chan, A quantitative model-independent method for global sensitivity analysis of model output. *Technometrics* **41**, 39-56 (1999).
39. W. M. Deen, *Analysis of transport phenomena*. (Oxford university press New York, 1998), vol. 2.
40. I. Pinilla-Macua, S. C. Watkins, A. Sorkin, Endocytosis separates EGF receptors from endogenous fluorescently labeled HRas and diminishes receptor signaling to MAP kinases in endosomes. *Proc Natl Acad Sci U S A* **113**, 2122-2127 (2016).
41. J. Schindelin *et al.*, Fiji: an open-source platform for biological-image analysis. *Nat Methods* **9**, 676-682 (2012).
42. U. Horzum, B. Ozdil, D. Pesen-Okvur, Step-by-step quantitative analysis of focal adhesions. *MethodsX* **1**, 56-59 (2014).
43. B. Moser, B. Hochreiter, R. Herbst, J. A. Schmid, Fluorescence colocalization microscopy analysis can be improved by combining object-recognition with pixel-intensity-correlation. *Biotechnol J* **12**, (2017).
44. K. Zuiderveld, Contrast Limited Adaptive Histogram Equalization. *Graphics Gems* **0**, 474-485 (1994).
45. S. Surve, S. C. Watkins, A. Sorkin, EGFR-RAS-MAPK signaling is confined to the plasma membrane and associated endorecycling protrusions. *J Cell Biol* **220**, (2021).
46. R. J. Reddy *et al.*, Early signaling dynamics of the epidermal growth factor receptor. *P Natl Acad Sci USA* **113**, 3114-3119 (2016).
47. K. Roepstorff *et al.*, Differential Effects of EGFR Ligands on Endocytic Sorting of the Receptor. *Traffic* **10**, 1115-1127 (2009).
48. F. T. Huang, D. Kirkpatrick, X. J. Jiang, S. Gygi, A. Sorkin, Differential regulation of EGF receptor internalization and degradation by multiubiquitination within the kinase domain. *Mol Cell* **21**, 737-748 (2006).
49. D. Rotin *et al.*, Sh2 Domains Prevent Tyrosine Dephosphorylation of the Egf Receptor - Identification of Tyr992 as the High-Affinity Binding-Site for Sh2 Domains of Phospholipase C-Gamma. *Embo J* **11**, 559-567 (1992).
50. E. Sandilands, V. G. Brunton, M. C. Frame, The membrane targeting and spatial activation of Src, Yes and Fyn is influenced by palmitoylation and distinct RhoB/RhoD endosome requirements. *J Cell Sci* **120**, 2555-2564 (2007).
51. N. A. Kulak, G. Pichler, I. Paron, N. Nagaraj, M. Mann, Minimal, encapsulated proteomic-sample processing applied to copy-number estimation in eukaryotic cells. *Nat Methods* **11**, 319-U300 (2014).
52. S. V. Surve *et al.*, Localization dynamics of endogenous fluorescently labeled RAF1 in EGF-stimulated cells. *Mol Biol Cell* **30**, 506-523 (2019).
53. S. Q. Zhang *et al.*, Shp2 regulates Src family kinase activity and Ras/Erk activation by controlling Csk recruitment. *Mol Cell* **13**, 341-355 (2004).
54. R. J. Nichols *et al.*, RAS nucleotide cycling underlies the SHP2 phosphatase dependence of mutant BRAF-, NF1-and RAS-driven cancers. *Nat Cell Biol* **20**, 1064-+ (2018).
55. T. S. Batth *et al.*, Large-Scale Phosphoproteomics Reveals Shp-2 Phosphatase-Dependent Regulators of Pdgf Receptor Signaling. *Cell Rep* **22**, 2784-2796 (2018).
56. M. Dance, A. Montagner, J. P. Salles, A. Yart, P. Raynal, The molecular functions of Shp2 in the Ras/Mitogen-activated protein kinase (ERK1/2) pathway. *Cell Signal* **20**, 453-459 (2008).

57. Y. Ren *et al.*, Critical role of Shp2 in tumor growth involving regulation of c-Myc. *Genes Cancer* **1**, 994-1007 (2010).
58. Y. Ren *et al.*, Roles of Gab1 and SHP2 in paxillin tyrosine dephosphorylation and Src activation in response to epidermal growth factor. *J Biol Chem* **279**, 8497-8505 (2004).
59. M. J. Lazzara *et al.*, Impaired SHP2-Mediated Extracellular Signal-Regulated Kinase Activation Contributes to Gefitinib Sensitivity of Lung Cancer Cells with Epidermal Growth Factor Receptor-Activating Mutations. *Cancer Res* **70**, 3843-3850 (2010).
60. C. M. Furcht, A. R. M. Rojas, D. Nihalani, M. J. Lazzara, Diminished functional role and altered localization of SHP2 in non-small cell lung cancer cells with EGFR-activating mutations. *Oncogene* **32**, 2346-2355 (2013).
61. Y. Wang, S. Pennock, X. M. Chen, Z. X. Wang, Endosomal signaling of epidermal growth factor receptor stimulates signal transduction pathways leading to cell survival. *Mol Cell Biol* **22**, 7279-7290 (2002).
62. M. Miaczynska, L. Pelkmans, M. Zerial, Not just a sink: endosomes in control of signal transduction. *Curr Opin Cell Biol* **16**, 400-406 (2004).
63. H. H. Ye, R. Kuruvilla, L. S. Zweifel, D. D. Ginty, Evidence in support of signaling endosome-based retrograde survival of sympathetic neurons. *Neuron* **39**, 57-68 (2003).
64. M. C. Good, J. G. Zalatan, W. A. Lim, Scaffold Proteins: Hubs for Controlling the Flow of Cellular Information. *Science* **332**, 680-686 (2011).
65. A. Fortian, A. Sorkin, Live-cell fluorescence imaging reveals high stoichiometry of Grb2 binding to the EGF receptor sustained during endocytosis. *J Cell Sci* **127**, 432-444 (2014).
66. M. M. Moasser, The oncogene HER2: its signaling and transforming functions and its role in human cancer pathogenesis. *Oncogene* **26**, 6469-6487 (2007).
67. Y.-X. Fan *et al.*, Acquired Substrate Preference for GAB1 Protein Bestows Transforming Activity to ERBB2 Kinase Lung Cancer Mutants. *J Biol Chem* **288**, 16895-16904 (2013).
68. F. Matalkah, E. Martin, H. Zhao, Y. M. Agazie, SHP2 acts both upstream and downstream of multiple receptor tyrosine kinases to promote basal-like and triple-negative breast cancer. *Breast Cancer Research* **18**, (2016).
69. H. Lu *et al.*, SHP2 Inhibition Overcomes RTK-Mediated Pathway Reactivation in KRAS-Mutant Tumors Treated with MEK Inhibitors. *Molecular Cancer Therapeutics* **18**, 1323-1334 (2019).
70. M. I. Kontaridis, X. Liu, L. Zhang, A. M. Bennett, Role of SHP-2 in Fibroblast Growth Factor Receptor-Mediated Suppression of Myogenesis in C2C12 Myoblasts. *Mol Cell Biol* **22**, 3875-3891 (2002).
71. B. S. Hendriks, L. K. Opresko, H. S. Wiley, D. Lauffenburger, Quantitative analysis of HER2-mediated effects on HER2 and epidermal growth factor receptor endocytosis - Distribution of homo- and heterodimers depends on relative HER2 levels. *J Biol Chem* **278**, 23343-23351 (2003).
72. Y. X. Fan, L. Wong, T. B. Deb, G. R. Johnson, Ligand regulates epidermal growth factor receptor kinase specificity - Activation increases preference for GAB1 and SHC versus autophosphorylation sites. *J Biol Chem* **279**, 38143-38150 (2004).
73. A. Kiyatkin *et al.*, Scaffolding protein Grb2-associated binder 1 sustains epidermal growth factor-induced mitogenic and survival signaling by multiple positive feedback loops. *J Biol Chem* **281**, 19925-19938 (2006).

74. D. Barua, J. R. Faeder, J. M. Haugh, Structure-based kinetic models of modular signaling protein function: Focus on Shp2. *Biophys J* **92**, 2290-2300 (2007).